Journal of Anatomy

J. Anat. (2012) **220**, pp423–434 doi: 10.1111/j.1469-7580.2012.01485.x

Packing a pinch: functional implications of chela shapes in scorpions using finite element analysis

Arie van der Meijden,[1] Thomas Kleinteich[2,3] and Pedro Coelho[1]

[1]*CIBIO, Centro de Investigação em Biodiversidade e Recursos Genéticos, Vairão, Portugal*
[2]*Friday Harbor Laboratories, University of Washington, Friday Harbor, WA, USA*
[3]*Zoology Department, Christian-Albrechts-Universität Kiel, Kiel, Germany*

Abstract

Scorpions depend on their pedipalps for prey capture, defense, mating and sensing their environment. Some species additionally use their pedipalps for burrowing or climbing. Because the pincers or chelae at the end of the pedipalps vary widely in shape, they have been used as part of a suite of characters to delimit ecomorphotypes. We here evaluate the influence of the different chela cuticular shapes on their performance under natural loading conditions. Chelae of 20 species, representing seven families and spanning most of the range of chela morphologies, were assigned to clusters based on chela shape parameters using hierarchical cluster analysis. Several clusters were identified corresponding approximately to described scorpion ecomorphotypes. Finite element models of the chela cuticulae were constructed from CT scans and loaded with estimated pinch forces based on *in vivo* force measurements. Chela shape clusters differed significantly in mean Von Mises stress and strain energy. Normalized FEA showed that chela shape significantly influenced Von Mises stress and strain energy in the chela cuticula, with Von Mises stress varying up to an order of magnitude and strain energy up to two orders of magnitude. More elongate, high-aspect ratio chela forms showed significantly higher mean stress compared with more robust low-aspect ratio forms. This suggests that elongate chelae are at a higher risk of failure when operating near the maximum pinch force. Phylogenetic independent contrasts (PIC) were calculated based on a partly resolved phylogram with branch lengths based on an alignment of the 12S, 16S and CO1 mitochondrial genes. PIC showed that cuticular stress and strain in the chela were correlated with several shape parameters, such as aspect ratio, movable finger length, and chela height, independently of phylogenetic history. Our results indicate that slender chela morphologies may be less suitable for high-force functions such as burrowing and defense. Further implications of these findings for the ecology and evolution of the different chela morphologies are discussed.

Key words: finite element analysis; independent contrasts; Scorpiones.

Introduction

Scorpions are a large and ancient group of chelicerates with close to 2000 described species (Fet et al. 2000) that have successfully adapted to a diversity of habitats on all continents except Antarctica. Despite occurring in a wide variety of habitats, scorpions have changed little in overall body plan since the Silurian (Dunlop et al. 2008). Their most notable features are the pedipalps, carrying the chelae (the 'pincers'), and the metasoma (the 'tail'), carrying the venomous telson (the 'stinger'). All these structures are used in prey subjugation and defense. The pedipalps are additionally used in mating, climbing and digging, and serve as a sensory array similar to the antennae of insects and crustaceans (Alexander, 1959; Fet et al. 2003).

The chelae are formed by the last two segments of the pedipalps; the manus or tibia, which contains the muscles and also forms the immovable finger, and the movable finger or tarsus. The movable finger is adducted by three muscle bundles in the chela manus (Gilai & Parnas, 1970). In addition, there is also a small closing muscle in the next segment (patella), which is connected to the movable finger by a long ligament (Snodgrass, 1952; Gilai & Parnas, 1970). The movable finger is abducted by the elastic recoil of resilin in the joint (Govindarajan & Rajulu, 1974; Sensenig & Shultz, 2004), opening the chela. The movable finger rotates

Correspondence
Arie van der Meijden, CIBIO, Centro de Investigação em Biodiversidade e Recursos Genéticos, Campus Agrário de Vairão, 4485-661 Vairão, Portugal. E: mail@arievandermeijden.nl

Accepted for publication *26 January 2012*
Article published online *23 February 2012*

around an axis defined by two joints, located on the median and lateral sides of the chela.

Despite conservancy in their ecological role as mostly terrestrial predators, scorpions have been known to have specific adaptations to certain environments. Several ecomorphotypes were recognized based on a qualitative review of the local scorpion faunas of sub-Saharan Africa (Lamoral, 1979) and North America (Polis, 1990). In these studies, the shape of the chelae is considered an important character in the delimitation of five putative ecomorphotypes. Robust chelae with a high muscle-filled manus and relatively shorter fingers that are reminiscent of chelae in durophagous crabs are ascribed to digging (fossorial) species. Sand-dwelling (psammophilous) species have more elongate chelae with long fingers. Species that hide in or under rocks (saxicoline) or bark (corticoline) have dorsoventrally compressed bodies and appendages including the chelae, to facilitate living in narrow spaces (Newlands, 1972). Actively foraging scorpions with slender bodies and appendages are sometimes considered an additional ecomorphotype, the errant ecomorphotype (Polis, 1990). Chelae of the errant ecomorphotype are similar to the chelae in psammophilous species. These different putative ecomorphotypes have never been quantitatively corroborated.

The described different morphologies change the functional properties of the chelae. The volume of the manus is largely determined by the amount of muscle in that segment, which partly determines the force a scorpion can produce with its chelae. As in durophagous crabs (Yamada & Boulding, 1998), the height of the manus relative to the length of the chela is therefore indicative of pinch force (Van der Meijden et al. 2010). The pinch force of a scorpion is further determined by the lever system that transfers the force from the muscles to the tips of the fingers of the chelae. The mechanical advantage of this lever system is very variable in scorpions. As the out-lever (the external part of the movable finger) of a first class lever system gets longer relative to the in-lever (the internal part of the movable finger, to which the muscles attach), the mechanical advantage of the lever system may increase speed at the cost of force (but see McHenry, 2011). Longer fingers may thus give the scorpion an advantage to catch elusive insect prey by increased closing speed or gape size. Since this arrangement makes the chelae relatively inefficient in producing high forces, such long-fingered chelae are feeble weapons to fend of predators. The robust chelae of fossorial species allow for more muscle to be packed into the chela and for a longer in-lever inside the chela manus, thus improving the mechanical advantage for force production. Newlands (1969, 1972) suggested that the large chelae may also be used in blocking the burrow, to keep out predators. Other authors have noted that scorpions with robust chelae use their sting less in prey incapacitation than scorpions with more slender chelae (Stahnke, 1966; McCormick & Polis, 1990), which suggests a trade-off between the chelae and the stinger in prey incapacitation. Although morphological characters of the chela are important in taxonomic studies, the functional implications of shape to the performance of the chela have received little attention. Knowledge on the functional consequences of different chela shapes, however, is crucial to understand their adaptive value and to identify functional demands during scorpion evolution. This report is the first evaluation of the functional implications of the shape of the chela cuticula in scorpions. We use 3-dimensional finite element models to estimate the stresses that the chela cuticula of different chela morphologies experience under biologically realistic force production.

Materials and methods

Species selection

A total of 20 species (Table 1) were selected from seven families to represent the range of chela morphology found in extant scorpions. Animals were selected based on availability through field collecting or the pet trade.

Morphological measurements

Morphological measurements were taken using digital calipers. Several preserved specimens were measured per species and average chela measurements were calculated. However, for some species only a single specimen was available. Morphological data are shown in Table 1. In addition to linear measurements, the curvature of the movable finger was determined using a custom MATLAB script (available from the corresponding author upon request). The ventral view of the chela movable finger was used to fit a circle to the inside and outside curve of the movable finger. The average radius of these two circles was then divided by the length of the movable finger to attain a size-independent metric of curvature. In addition the angle between the axis of rotation of the movable finger to the line connecting the tip of the movable finger to the center of the axis of rotation was calculated (α in Fig. 1C). The angle between the in-lever and out-lever of the movable finger was calculated as the angle between the plane defined by the fingertip (T), the median joint (MJ) and lateral joint (LJ), and the plane defined by the insertion point of the muscles (MI), the median joint (MJ) and lateral joint (LJ) (see Fig. 1A).

To group similarly shaped chelae, we performed a clustering analysis on normalized linear measurements of the chela. Manus height, manus width and length of movable finger were normalized by division with total chela length. These normalized data were used to identify clusters of similarly shaped chelae. Clustering analysis was performed in R (R Development Core Team). The data were clustered hierarchically using the Ward method based on Euclidian distance between species. Clusters in the data were also identified using the k-clustering method, with the variable k (number of clusters) being identified through the expectation maximization algorithm as implemented in the R package MCLUST.

Table 1 Species used in this study, and measured and derived morphological parameters. Asterisk indicates measurements from a similar-size specimen.

Species		Family	Measured specimens	Total length (mm)	Prosoma length (mm)	Chela length (mm)	Normalized width	Normalized height	Normalized movable finger length	Aspect ratio	Mechanical advantage	Angle in-lever-out-lever (degrees)	Angle out-lever – axis of rotation (degrees)	Measured max force (N)	Predicted force (N)	Curvature movable finger	Max. Von Misses stress (Pa) – scaled	Mean Von Misses stress (Pa) – scaled	Total strain energy (J) corrected	12S accession number	Accession number 16S	Accession number CO1
Androctonus amoreuxi	(Audouin, 1826)	Buthidae	8	81.8	10.21	19.45	0.24	0.27	0.64	3.34	4.69	101.2	77.0	2.0*	3.75	2.35	1.43E+08	3.99E+06	1.67E-06	JQ423120	JQ514228	JQ514246
Androctonus australis	(Linnaeus, 1758)	Buthidae	15	78.4	10.12	19.02	0.28	0.31	0.66	3.53	4.29	85.8	80.6	2.8*	3.3	1.81	1.15E+08	5.04E+06	1.78E-06	JQ423124	JQ514232	JQ514250
Bothriurus chilensis	(Molina, 1782)	Bothriuridae	1	35.0	4.39	6.18	0.31	0.38	0.53	2.53	3.56	56.4	79.5		0.53	1.86	1.06E+08	2.10E+06	4.14E-07	Missing	JQ514230	Missing
Caraboctonus keyserlingi	Pocock, 1893	Iuridae	8	35.6	5.84	8.66	0.32	0.34	0.58	3.02	4.35	104.3	63.2		0.91	2.50	2.30E+08	3.53E+06	1.18E-06	JQ423123	JQ514231	JQ514249
Chactas sp.		Chactidae	1	36.5	6.51	10.58	0.36	0.50	0.60	2.07	3.18	66.7	70.2		2.1	1.75	3.20E+07	1.85E+06	2.78E-07	JQ423128	JQ514239	JQ514255
Euscorpius flavicaudis	(DeGeer, 1778)	Euscorpiidae	1	26.7	4.92	8.44	0.22	0.37	0.57	3.56	3.89	100.7	56.4		0.41	1.91	3.92E+07	2.04E+06	4.92E-07	JQ423126	JQ514237	JQ514253
Grosphus flavopiceus	Kraepelin, 1900	Buthidae	10	105.2	11.18	20.55	0.26	0.26	0.59	3.85	5.01	124.3	79.7	0.9	3.66	1.61	9.54E+07	3.92E+06	2.02E-06	JQ423127	JQ514238	JQ514254
Hadogenes paucidens	Pocock, 1896	Liochelidae	12	130.5	14.63	26.83	0.18	0.34	0.50	2.96	3.24	107.9	57.4	18.2	12.92	2.17	7.32E+08	3.14E+06	7.53E-07	JQ423130	Missing	JQ514257
Hadrurus arizonensis	Ewing, 1928	Iuridae	9	86.9	12.69	21.1	0.22	0.34	0.70	3.13	5.4	76.4	78.8	3.4*	7.83	2.20	1.43E+08	4.65E+06	2.33E-06	JQ423129	JQ514240	JQ514256
Hoffmannius sp.		Vaejovidae	1	33.2	4.36	6.99	0.17	0.19	0.70	5.64	7.5	62.4	83.1		0.09	2.45	1.14E+07	7.71E+06	9.14E-06	JQ423133	JQ514243	Missing
Hottentota gentili	(Pallary, 1924)	Buthidae	10	85.8	9.94	20.59	0.18	0.19	0.69	4.49	6.03	106.4	82.3	1.2*	1.84	2.05	4.34E+08	7.88E+06	5.95E-06	JQ423119	JQ514227	JQ514245
Iurus dufoureius	(Brullé, 1832)	Iuridae	1	64.8	10.01	20.95	0.26	0.34	0.61	3.03	4.03	71.9	72.5		4.21	1.93	2.85E+08	2.95E+06	6.69E-07	JQ423125*	JQ514235*	JQ514252*
Leiurus quinquestriatus	Ehrenberg, 1828	Buthidae	9	75.8	9.22	17.22	0.15	0.17	0.72	6.55	7.52	64.6	82.3	0.7*	0.48	2.03	2.28E+08	1.51E+07	1.44E-05	JQ423131	JQ514241	JQ514258
Liocheles australasiae	(Fabricius, 1775)	Liochelidae	1	21.6	4.02	7.3	0.18	0.37	0.42	2.81	3	55.5	66.7		0.35	1.42	2.04E+07	2.30E+06	3.79E-07	Missing	JQ514233	DQ127506
Opisthacanthus madagascariensis	Kraepelin, 1894	Liochelidae	7	42.8	7.46	14.31	0.23	0.42	0.54	2.31	3.02	97.8	59.4	2.9*	2.71	1.84	4.13E+08	1.41E+06	1.89E-07	Missing	JQ514236	Missing
Opistophthalmus boehmi	(Kraepelin, 1896)	Scorpionidae	6	48.2	7.38	11.69	0.29	0.50	0.59	2.16	3.28	72.6	70.2		2.86	1.89	5.41E+07	1.79E+06	2.13E-07	JQ423122	Missing	JQ514248
Orthochirus innesi	Simon, 1910	Buthidae	1	30.0	3.8	5.04	0.18	0.20	0.65	5.18	5.09	62.1	86.0		0.08	2.73	7.04E+07	4.57E+06	3.00E-06	JQ423118	JQ514226	JQ514244
Pandinus cavimanus	(Pocock, 1888)	Scorpionidae	3	81.6	15.74	26.5	0.28	0.62	0.66	1.45	3.1	54.1	75.8	24.5	36.5	2.15	1.96E+08	1.92E+06	2.06E-07	AY156550	JQ514234*	JQ514251*
Parabuthus transvaalicus	Purcell, 1899	Buthidae	5	88.0	9.38	13.56	0.23	0.24	0.66	4.99	5.82	74.8	83.2	0.4	1.18	2.51	7.78E+07	4.25E+06	2.01E-06	JQ423121	JQ514229	JQ514247
Scorpio fuliginosus	(Pallary, 1928)	Scorpionidae	8	n.a.	8.34	11.88	0.33	0.64	0.57	2.89	2.54	62.8	67.9	6.3*	2.7	1.57	1.93E+08	1.09E+06	1.69E-07	JQ423132	JQ514242	JQ514259

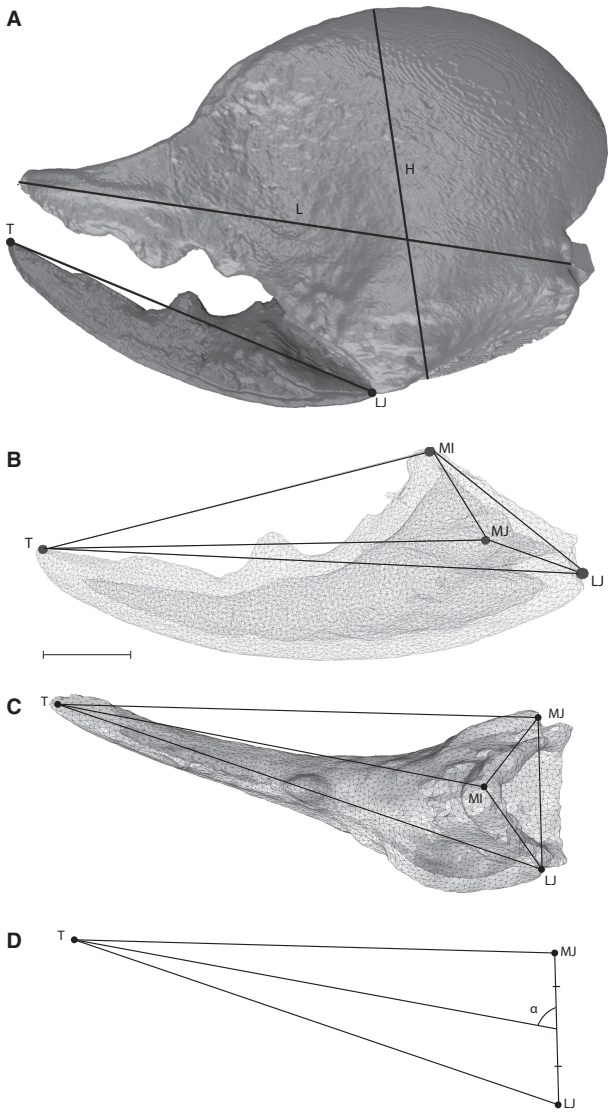

Fig. 1 (A) Linear measurements on the chela Length (L), Height (H), movable finger length (T-LJ). (B,C) Measurements on chela movable finger, exemplified on the movable finger of *Pandinus cavimanus*. (B) Side view of a transparent wireframe mesh. (C) Dorsal view, solid wireframe mesh. (D) Dorsal view showing angle (α) between center of joint axis (LJ-MJ) and finger tip (T). LJ, lateral joint; MJ, medial joint; MI, muscle insertion; T, tip. The line LJ-MJ is the axis of rotation for the movable finger.

Pinch force measurement and estimation

Live animals were maintained as described in Van der Meijden et al. (2010). *In vivo* pinch forces were measured using either a Kistler force transducer (type 9203; Kistler Inc., Switzerland) mounted on a purpose-built holder (see Herrel et al. 1999) or a similar setup with a Sauter FH20 external force sensor (Sauter Ltd., Germany). Measurements were made in a climate-controlled room at 23–24 °C. During pinch force measurements, scorpions were restrained between sponge pads in which a cutout was made to accommodate the body, or by placing a padded clamp over the last segments of the metasoma to allow safe handling. Most specimens pinched readily, but some were stimulated to pinch by stroking the inside of the chela with the tip of a pair of tweezers. Five trials were performed, separated by at least 1 day. Only the maximum force per chela was used for further analyses.

Live specimens were not available for all species included in this study to measure pinch forces. Further, some species were too small for accurate measurements using parallel plates. For species for which *in vivo* pinch forces were not available, we estimated pinch forces based on the aspect ratios of the chelae. Chela aspect ratio was previously demonstrated to be a good predictor of pinch forces ($R^2 = 0.90$; Van der Meijden et al. 2010). We further expanded the dataset from Van der Meijden et al. (2010) to comprise 170 specimens from 20 species, representing four families (Buthidae, Iuridae, Liochelidae, Scorpionidae; data to be published elsewhere). The maximum pinch forces were $\log_{10}$-transformed, and standardized for the size of the animal by regression of the forces against $\log_{10}$-transformed prosoma length. Body mass or total length cannot be used as a proxy for overall size in scorpions, as both can change significantly depending on feeding state. The residuals were then regressed against the aspect ratio of the chela (length/height). Pinch force was predicted based on a line function that was fit to the data using least squares ($R^2 = 0.54$, Pearson's correlation coefficient −0.73). The resulting predicted maximum pinch forces are shown in Table 1.

Specimen scanning and model reconstruction

We CT-scanned the chelae of the specimens with a Skyscan 1076 micro CT scanner from the Small Animal Tomographic Analysis Facility at the Seattle Children's Research Institute in Seattle, WA, USA. The specimens were scanned at a source voltage of 31 kV and a source currency of 187 μA at 35 μm resolution. The raw X-ray images that were recorded during CT imaging were then converted with the software tool NRECON (Skyscan) into a volumetric dataset that consisted of a stack of TIFF image files.

The volumetric dataset was imported into the 3D visualization software AMIRA 5.3.3 (Visage Imaging). In AMIRA, we used the *Labels* function to separate the cuticles of the scorpion chelae from the remainder structures that were visible in the CT dataset. We further separated the cuticle of the manus from the cuticle of the movable finger and saved them as two separate materials in the *Labels* dataset that is generated during segmentation in AMIRA. Based on the materials in the *Labels* dataset, we calculated polygonal surfaces for the manus and the movable finger with AMIRA. The resulting surfaces were then edited in the *Surface Editor Mode* of AMIRA to distribute the polygons equally over the surface, reduce the total number of polygons, and fix occurring intersections between polygons that were in close proximity to each other. For each specimen, we measured the surface area and the volume with AMIRA. We then converted the polygonal surfaces to solid models that were built from tetrahedral elements, i.e. the elements were defined by four nodes. The number of elements ranged from 20 000 to 2.4 million depending on the size of the specimen (Table 2).

Finite element analysis

The solid models for the manus and the finger of each specimen were imported as IDEAS files into the finite element modeling and analyzing software MARC MENTAT 2005 R3 (MSC software).

Table 2 Details of the chela models used in this study.

Species	Modeled Chela	# Elements Manus	# Elements finger	Surface area Manus (m^2)	Surface area finger (m^2)	Total surface area (m^2)	Force : total surface area (N m^{-2})	Surface scaling factor	Scaled force (N)	Volume manus (m^3)	Volume finger (m^3)	Total volume (m^3)	Scaled force : total volume$^{1/6}$ (N $m^{-3/6}$)	Energy scaling factor
Androctonus amoreuxi	Left	602.606	329.656	3.54E−04	7.42E−05	4.28E−04	9.21E+03	0.284	1.07	4.54E−08	1.97E−08	6.51E−08	16.83	0.103
Androctonus australis	Left	473.202	339.943	3.36E−04	8.59E−05	4.22E−04	9.49E+03	0.329	1.08	4.07E−08	1.66E−08	5.73E−08	17.44	0.100
Bothriurus chilensis	Left	178.886	58.392	5.33E−05	9.45E−06	6.27E−05	9.52E+03	0.305	0.16	2.79E−09	6.71E−10	3.46E−09	4.14	0.419
Caraboctonus keyserlingi	Left	76.686	28.877	8.50E−05	1.62E−05	1.01E−04	9.00E+03	0.285	0.26	5.12E−09	1.12E−09	6.24E−09	6.07	0.286
Chactas sp.	Left	225.370	109.687	1.74E−04	2.90E−05	2.03E−04	1.30E+04	0.246	0.52	1.51E−08	3.87E−09	1.90E−08	10.03	0.173
Euscorpius flavicaudus	Right	127.830	43.706	8.10E−05	1.49E−05	9.59E−05	8.76E+03	0.605	0.25	6.02E−09	1.31E−09	7.33E−09	5.69	0.305
Grosphus flavopiceus	Right	732.718	301.907	3.40E−04	6.55E−05	4.05E−04	9.71E+03	0.284	1.04	5.38E−08	1.49E−08	6.87E−08	16.27	0.107
Hadogenes paucidens	Right	881.421	375.594	7.78E−04	1.35E−04	9.13E−04	1.20E+04	0.182	2.35	1.37E−07	3.40E−08	1.71E−07	31.53	0.055
Hadrurus arizonensis	Left	786.112	460.487	3.66E−04	1.07E−04	4.73E−04	6.54E+03	0.155	1.22	4.71E−08	1.92E−08	6.63E−08	15.72	0.110
Hoffmannius sp.	Left	18.582	6.795	2.35E−05	3.94E−06	2.74E−05	4.32E+03	0.787	0.07	1.88E−09	2.34E−10	2.11E−09	2.04	0.850
Hottentota gentili	Right	831.107	305.133	2.74E−04	7.93E−05	3.53E−04	6.28E+03	0.487	0.90	3.33E−08	1.26E−08	4.59E−08	15.00	0.116
Iurus dufoureius	Left	906.933	476.716	4.56E−04	1.07E−04	5.63E−04	1.05E+04	0.344	1.45	7.07E−08	1.98E−08	9.05E−08	21.61	0.080
Leiurus quinquestriatus	Left	129.136	97.081	1.40E−04	4.44E−05	1.84E−04	3.71E+03	1.000	0.48	1.05E−08	4.53E−09	1.50E−08	9.60	0.181
Liocheles australasiae	Right	59.974	18.467	6.30E−05	9.49E−06	7.24E−05	1.00E+04	0.545	0.19	2.95E−09	6.77E−10	3.63E−09	4.91	0.354
Opisthacanthus madagascariensis	Right	410.352	254.362	2.76E−04	4.42E−05	3.20E−04	1.20E+04	0.303	0.82	3.23E−08	1.02E−08	4.25E−08	13.92	0.125
Opistophthalmus boehmi	Left	210.280	185.500	1.88E−04	3.96E−05	2.27E−04	1.14E+04	0.208	0.60	2.32E−08	6.05E−09	2.93E−08	10.72	0.162
Orthochirus innesi	Left	14.562	5.616	1.47E−05	4.15E−06	1.89E−05	5.16E+03	0.659	0.05	6.00E−10	2.43E−10	8.43E−10	1.74	1.000
Pandinus cavimanus	Left	1.671.634	637.596	1.47E−03	3.64E−04	1.83E−03	1.04E+04	0.129	4.71	2.71E−07	8.02E−08	3.51E−07	56.02	0.031
Parabuthus transvaalicus	Right	374.713	160.650	1.75E−04	2.29E−05	1.98E−04	3.93E+03	0.329	0.39	1.12E−08	4.48E−09	1.57E−08	7.78	0.223
Scorpio fuliginosus	Left	919.610	211.896	5.40E−04	6.68E−05	6.07E−04	7.89E+03	0.376	1.02	4.69E−08	9.29E−09	5.62E−08	16.41	0.106

Because the gapes between manus and finger in different specimens differed, we had to manually adjust the gape angles in MARC MENTAT. For this, we oriented the models to align the axis that connects the centers of the two joints between manus and finger with the origin of the coordinate system in MARC MENTAT. This allowed us to rotate the manus and the finger independently without dislocation at the joint and to set the gape angle at 15° for each specimen. For a more realistic estimate on the reaction forces that act on the joint between manus and finger under load, we declared elements of the manus and of the finger to be on two different *Contact Bodies* and we assigned the nodes in the joint area as *Contact Areas*. Within *Contact Areas*, MARC MENTAT treats elements that are closer to each other than a defined threshold value (1/20 of the size of the smallest element) as contacting elements. For the finite element analysis, the contact between finger and manus was treated as two-sided (i.e. the finger contacts the manus and vice versa) and we used the *Optimized Contact Constraints* option to avoid penetration between finger and manus.

We treated the cuticle of the chelae as isotropic material with a Young's modulus of 7 GPa and a Poisson's ratio of 0.3. Young's moduli of arthropod cuticle have been reported to cover a wide range from 0.1 to 20 GPa (Vincent & Wegst, 2004). Although the value for the Young's modulus of 7 GPa that we have chosen is only a estimate based on the assumption that scorpion chelae have a rather hard cuticle and absolute output values are biased by this estimate, finite element modeling provides a powerful tool for comparisons between species, even if the exact material attributes are not available (Dumont et al. 2009).

We applied the following constraints (in MARC MENTAT *Boundary Conditions*) to the models: (i) all nodes in the areas of muscle attachment on the manus and the finger were fixed to prevent translation or rotation for each degree of freedom; (ii) bite force was distributed over four nodes on each, the finger and the manus, and modeled as point loads. We ran two separate analyses for each specimen. For the first constraint (I) we used the measured and predicted force values in Table 1 as bite force (absolute approach with unscaled results). For the second (ii) we calculated the force per surface area ratios for each specimen and applied bite forces that were scaled to fit the smallest force per surface area ratio in our specimen sample (comparative approach with scaled results).

We used three different measures to quantify the biting performance of scorpion chelae with finite element analysis: (i) maximum Von Mises stress; (ii) mean Von Mises stress, and (iii) total strain energy. Von Mises stress is used as a measure of how close a material is to failure. Areas in the chelae with higher Von Mises stresses are closer to failure than areas that experience lower Von Mises stresses. However, maximum Von Mises stresses can be hard to interpret in finite element models because the constrained areas (i.e. the applied point loads and fixed nodes) tend to show artificially high Von Mises stresses (Dumont et al. 2009). Mean Von Mises stress is supposed to be a more reliable measure of overall performance based on the assumption that chelae shapes that perform better under load will show lower Von Mises stresses over each node compared with shapes that perform poorly. Total strain energy reflects the amount of work that is used for deformation of the shapes, rather than for biting. It is assumed that scorpions that perform better during biting exhibit lower total strain energies, i.e. their chelae deform less under load. Von Mises stress and total strain energy are standard outputs of MARC MENTAT.

Because in the comparative approach, all models had identical force to surface area ratios, Von Mises stresses were directly comparable between species (Dumont et al. 2009). However, total strain energy scales with the volume of the models instead of the surface area. To make the calculated values for total strain energy directly comparable between species, we calculated an energy scaling factor that was based on the specimen with the lowest force per sixth root of the volume ratio. Volume corrected total strain energies were then calculated by multiplication of the square of the energy scaling factor with the raw total strain energies. A detailed derivation of the equations to scale finite element models was provided by Dumont et al. (2009).

The numbers of elements for each specimen varied considerably despite similar edge lengths of the elements (Table 2). This was caused by the different sizes of the specimens. To estimate the effect of mesh-size on the performance parameters evaluated herein, we re-meshed the finite element model of the specimen with the least amount of elements (*Orthochirus innesi*), to generate models with eight and 64 times the number of the original elements, respectively (Supporting Information Table S1). Finite element analysis with the re-meshed datasets showed only slight variations in mean Von Mises stress and total strain energy that are negligible compared with the interspecific variation. This indicates that mean Von Mises stress and total strain energy can be used for comparisons among datasets that consist of different amounts of elements; maximum Von Mises stress increases in the re-meshed models, which is likely to be caused by an increased localization of point loads.

Phylogenetic analysis and independent contrasts

Total DNA was extracted from fresh or preserved (96% ethanol) muscle tissue using standard high-salt protocols (Bruford et al. 1992). A fragment of the mitochondrial cytochrome C oxidase, subunit I (*COI*) gene was amplified by PCR using primers LCO1490 and HCO2198 (Folmer et al. 1994) or primers in the same locus based on an alignment of *CO1* sequences available in GenBank as of 4-2011. The sequence of these primers was: forward (5′-WTYCTACIAATCAYAARGATATTGG-3′) and reverse (5′-TAMACYTCIGGGTGWCCAAAAAAYCA-3′). A fragment of the mitochondrial *16S* rDNA gene was amplified using the primers LR-J-12887 (Simon et al. 1994) as forward primer, and a scorpion-specific reverse primer (Gantenbein et al. 2000). *12S* primers were designed based on available *12S* sequences in GenBank: forward primer 12S_F_AvdM (5′-AGAG-TGACGGGCAA-TATGTG-3)′ and reverse primer 12s_r_AvdM (5′-CAGCGGCTGC-GGTTATAC-3′).

Purified PCR templates were sequenced using dye-labeled dideoxy terminator cycle sequencing on an ABI 3130 automated DNA sequencer or on an ABI 3730XL at Macrogen Inc. using the corresponding PCR primers. Chromatograms were checked and when necessary corrected using FINCHTV, version 1.4.0 (Geospiza, Inc., USA; http://www.geospiza.com). The obtained DNA sequences were aligned using MEGA 5 (Tamura et al. 2011). The coding sequence of *CO1* was aligned based on the translated amino acid sequence, and *12S* and *16S* rRNA sequences were aligned using Muscle (Edgar, 2004) as incorporated into MEGA 5 using the default settings.

Two methods of phylogenetic analysis, maximum likelihood (ML) and Bayesian inference (BI), were conducted using PHYML, version 3.0.1 (Guindon & Gascuel, 2003) and MRBAYES 3.1.2

(Ronquist & Huelsenbeck, 2003), respectively. The best fit models of nucleotide evolution were determined under the Akaike information criterion in JMODELTEST 0.1.1 (Posada, 2008). Nodal support for the topologies recovered in the ML analyses was obtained with 1000 bootstrap replicates. The BI analyses were run with 5 000 000 generations, sampling trees every 10th generation (and calculating a consensus tree after omitting the first 125 000 trees). Log likelihood scores for the remaining trees were graphed in TRACER 1.5 (http://beast.bio.ed.ac.uk/Tracer) and checked for appropriateness of the burnin-period.

Phylogenetic analysis of our molecular dataset did not contradict the current taxonomic relationships. Since phylogenetic reconstruction based on the combined alignment did not resolve all interfamilial relationships; for further analysis, the relationships between family level clades were changed to a star topology (by setting those branch lengths to zero). We grouped members of the same family together based on the taxonomy provided by Prendini & Wheeler (2005). Since our phylogenetic reconstruction of the relationships within the family Buthidae were well resolved and received high bootstrap support, we did not make any changes within the Buthidae. The full alignment was then used to produce a ML estimate (GTR+I+G) of the branch lengths with MEGA 5. The resulting phylogram was used to calculate phylogenetic independent contrasts of chela shape measurements and performance parameters using Phylocom (Webb et al. 2008). To control for an effect of the lack of support for interfamilial relationships, we also performed an independent contrast analysis on only the representatives of the Buthidae family, for which our molecular data provided good support.

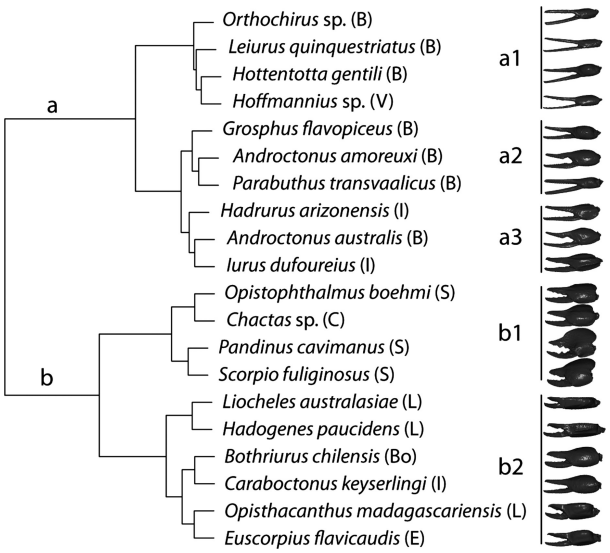

Fig. 2 Hierarchical clustering of chela shapes based on movable finger length, manus width and height, normalized for chela length. Cluster a contains the more elongate chela morphologies, cluster b contains the more robust chelae. Clusters a1, a2 and a3 have progressively smaller aspect ratios. Cluster b1 contains short strong chelae, whereas cluster b2 contains more flattened morphologies, typical of species that live in rock crevices and under bark.

Results

Clustering analysis

The expectation maximization algorithm found eight clusters with two or three species per cluster in the normalized linear chela measurements, showing significant structure in the dataset. All data clustering results are shown in Fig. 2. The chela shape data divide the dataset in two equal sized clusters, named cluster a and b. These clusters are further subdivided, and five of the subclusters were named a1–a3 and b1–b2. These clusters were not those selected using the expectation maximization algorithm (which selected eight smaller clusters), but more inclusive clusters were chosen as the authors believe them to better correspond with described ecomorphological types of chela morphology. Mann–Whitney tests were conducted to test differences in morphological and performance-related traits between all named clusters. The results of these tests can be found in Table 3. Of the normalized chela measurements that were used to define the clusters, only chela width did not significantly differ between the major clusters a and b. Subcluster b2, corresponding roughly with Lamoral's (1979) infrasaxicolous, lithosaxicolous and infracorticolous types, differed significantly from all other subclusters in chela height and movable finger length. There was no statistical difference between any of the clusters in chela length relative to the length of the prosoma (the latter being a good indicator of overall size).

Finite element analysis

Absolute approach

Under realistic loading conditions (i.e. the applied point loads corresponded to either actually measured *in vivo* bite forces or bite force estimates based on chela aspect ratio) maximum Von Mises stress, mean Von Mises stress, and total strain energy differed between species by several orders of magnitude (Table 1). This is in part accounted for by the different sizes of the specimens. Maximum Von Mises stress was highest in *Hadogenes paucidens* (7.32e8 Pa) and lowest in *Liocheles australasiae* (3.76e7 Pa). Mean Von Mises stress varied between 2.89e6 Pa in *Scorpio* and 3.64e7 Pa in *Hadrurus arizonensis*. Total strain energy was lowest in the very small *Orthochirus* (7.62e−6 J) and highest in the largest specimen included in this study, *Pandinus cavimanus* (1.25e−2 J).

Comparative approach

Scaling of the models based on surface area (for Von Mises stress) and volume (for total strain energy) allowed us to remove the effects of the size of the specimens from the analysis and to reveal the impacts of the different shapes on the performance. In our sample, the short-fingered species *Scorpio fuliginosus* and *Ophistacanthus madagascariensis* showed the least overall deformation under load,

Table 3 Mann–Whitney tests of statistical difference between named clusters of morphological and performance parameters. *P*-values higher than 0.05 are shown in grey.

	Chela width						
	a	b	a1	a2	a3	b1	b2
Chela height	a	0.052					
	b	1.1e−05					
	a1			0.057	0.057	0.029	0.067
	a2		0.057		0.700	0.057	0.714
	a3		0.057	0.100		0.057	0.905
	b1		0.029	0.057	0.057		0.114
	b2		0.010	0.024	0.024	0.010	
	Movable finger length						
	a	b	a1	a2	a3	b1	b2
Mechanical advantage	a	2.06e−04					
	b	4.3e−05					
	a1			0.114	0.629	0.057	0.010
	a2		0.114		0.700	0.400	0.024
	a3		0.114	0.400		0.114	0.024
	b1		0.029	0.057	0.057		0.019
	b2		0.010	0.024	0.095	0.352	
	a	b	a1	a2	a3	b1	b2
Angle out-lever/Joint axis	a						
	b	1.30e−04					
	a1						
	a2		0.400				
	a3		0.057	0.700			
	b1		0.029	0.050	0.108		
	b2		0.010	0.048	0.095	0.109	
	Chela aspect ratio						
	a	b	a1	a2	a3	b1	b2
Relative chela lengths	a	1.30e−04					
	b	0.218					
	a1			0.200	0.100	0.057	0.024
	a2		1.000		0.200	0.057	0.048
	a3		0.400	0.700		0.057	0.167
	b1		0.686	0.400	0.114		0.067
	b2		0.914	0.714	0.381	0.352	
	Strain energy (corrected)						
	a	b	a1	a2	a3	b1	b2
Von Mises stress	a	4.3e−05					
	b	8.7e−05					
	a1			0.057	0.057	0.029	0.010
	a2		1.000		1.000	0.057	0.024
	a3		0.857	0.268		0.057	0.095
	b1		0.686	1.000	0.629		0.067
	b2		0.762	0.714	0.905	0.610	

expressed in the lowest values for total strain energy. Conversely, species with elongated fingers such as *Hoffmannius* sp. and *Leiurus quinquestriatus* showed the most pronounced deformations of the chelae. The same pattern also emerged for mean Von Mises stress; *L. quinquestriatus* encountered the highest mean Von Mises stresses and *Scorpio* the lowest values. Maximum Von Mises stress was highest in *Hadogenes paucidens* and lowest in *Hoffmannius*. However, this is most likely caused by the presence of artificially high point loads in some of our models and the pattern of highest stresses in *H. paucidens*; the lowest stresses in *Hoffmannius* are not reflected by the plots of Von Mises stress over the 3D surfaces (Fig. 3).

The fingers of the chela act under load like a beam, i.e. they experience tensile stress along the edge where the load is applied and stress by compression along the edge opposite the load; between the compressed and tensioned edges lies a neutral axis with low stresses (Fig. 3). In species with slender, elongated fingers, the stresses on the movable part are similar to the counteracting fixed finger. In species with short chelae (e.g. *Scorpio*, *Pandinus cavimanus*), the roughly triangular shape of the fixed finger in lateral view tends to reduce the stress by compression on the edge opposite to the load. This results in an asymmetric stress distribution with higher stresses in the movable finger than in the fixed finger. The major clades a and b differed significantly in mean Von Mises stress and (size corrected) strain energy. As the Mann–Whitney test is based on ranking of the values, small datasets, such as the subclusters in this study, can be ordered in a limited number of ways. This leads to a tendency to converge on a small number of *P*-values, which accounts for the recurring value of some of the *P*-values in Table 3. In addition, we also tested for differences in the angle between the in-lever and the out-lever of the movable finger between the clusters, but found no statistically significant differences.

Phylogenetic analysis and independent contrasts

The total aligned dataset consisted of 1534 positions for 20 species. Bootstrap support was high within the Buthidae, but interfamilial relationships could not be recovered with high support (not shown). Branch lengths were therefore calculated starting with a phylogeny with a polytomy uniting all family level clades (Fig. 4).

The phylogenetic independent contrasts (Table 4) show that both mean Von Mises stress and strain energy correlate highly with several aspects of chela morphology, including size-corrected height, width, out-lever length, aspect ratio, mechanical advantage, and the ratio of the length of the movable finger to the distance between the joints. This corresponds with the observation from the clustering analysis that more elongate chelae experience higher stresses in the cuticula. Noteworthy is that the angle that the main axis of the movable finger makes with its axis of rotation is posi-

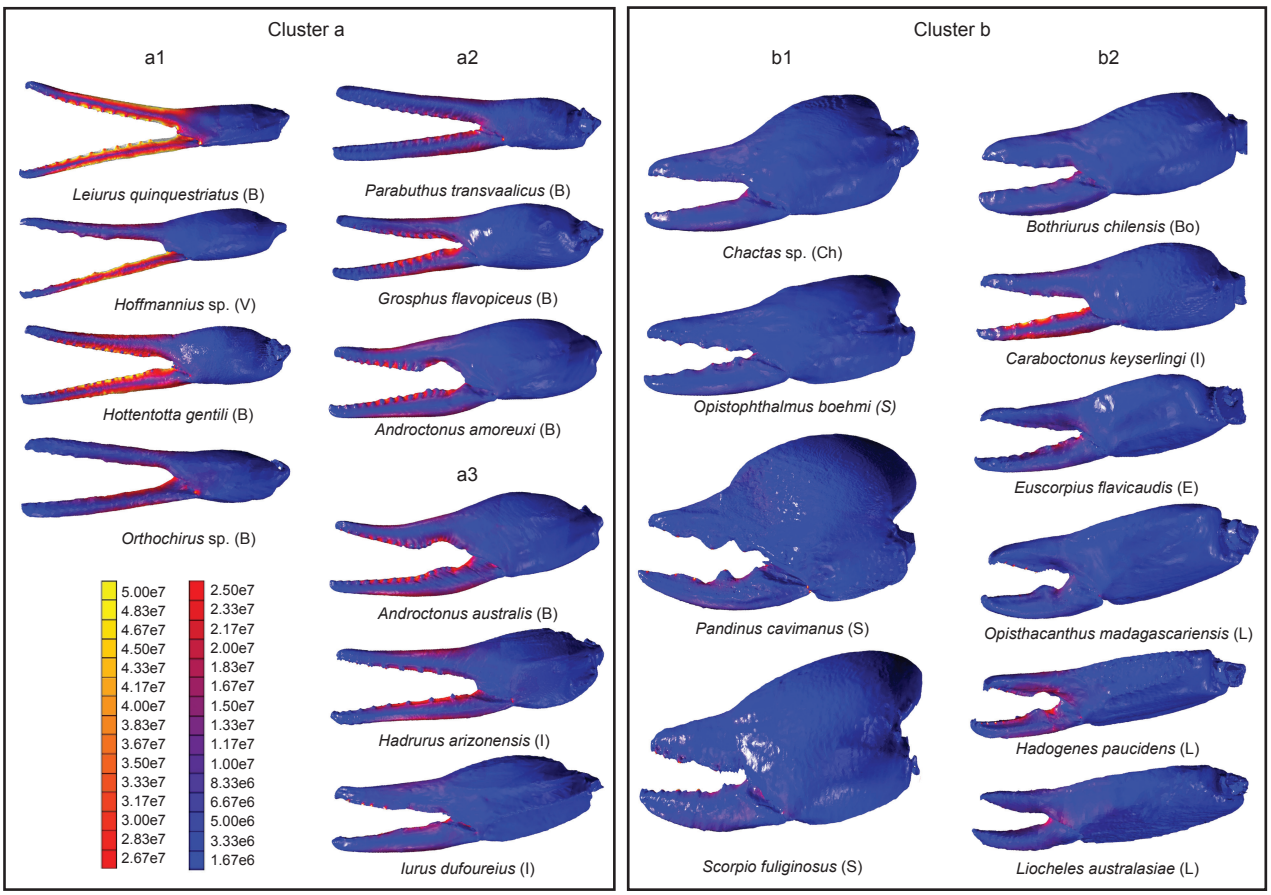

Fig. 3 FEA models with calculated Von Mises stress visualized as colors. Despite producing much less force, chelae with a high aspect ratio and long fingers (cluster a), experience much higher stresses than the more robust chelae of cluster b. High deformation can be seen in *Leiurus quinquestriatus*. High stresses indicate a risk of breakage, and the long-fingered chelae of cluster a are therefore at more at risk of breaking their fingers when exerting their maximum force.

tively correlated with the length of the movable finger ('out-lever' in Table 4), approaching a 90° angle for relatively longer fingers such as those of *Orthochirus*, *Hottentotta* and *Parabuthus*. Less surprising is that AR is highly correlated with the mechanical advantage of the chela. Neither mean Von Mises stress or strain energy correlated significantly with the angle between the in- and out-levers, the angle the out-lever makes with the axis of rotation, or the curvature of the finger. This may indicate that these variables are independent of the performance of the chela in resisting stresses during pinching and may be relevant for another function. The PIC analysis of the Buthidae only also showed high correlation coefficients for mean Von Mises stress and strain energy with aspect ratio, mechanical advantage, and the ratio of finger length to the distance between joints EJ–MJ (0.79, 0.88, 0.91, respectively, for both Von Mises stress and strain energy).

Discussion

To provide a basis for comparing the FEA results for similarly shaped chelae, we carried out a cluster analysis. In the hierarchical cluster analysis, we identified clusters which corresponded in part with previously described ecomorphotypes. The major clusters differed significantly in stress and bending energy, with the more elongate chela forms experiencing much higher stresses and deformations (for which bending energy is a metric). Phylogenetic independent contrasts also show that stress and deformation parameters correlate highly with chela shape parameters. Despite the lack of a fully resolved molecular phylogeny for the taxa in this study, the PIC analysis strongly indicates that chela shape and performance are correlated independently of phylogenetic history.

The clustering analysis revealed a significant structure in the limited number of normalized measurements used. Although the expectation maximization algorithm found up to eight clusters in the data, we chose a more conservative number of five clusters from the hierarchical cluster analysis. Several of the clusters roughly corresponded to ecomorphotypes qualitatively described in the literature (Newlands, 1972; Lamoral, 1979; Polis, 1990), although those ecomorphotypes are based on the whole body form, not merely the chelae. The elongate chelae in cluster a,

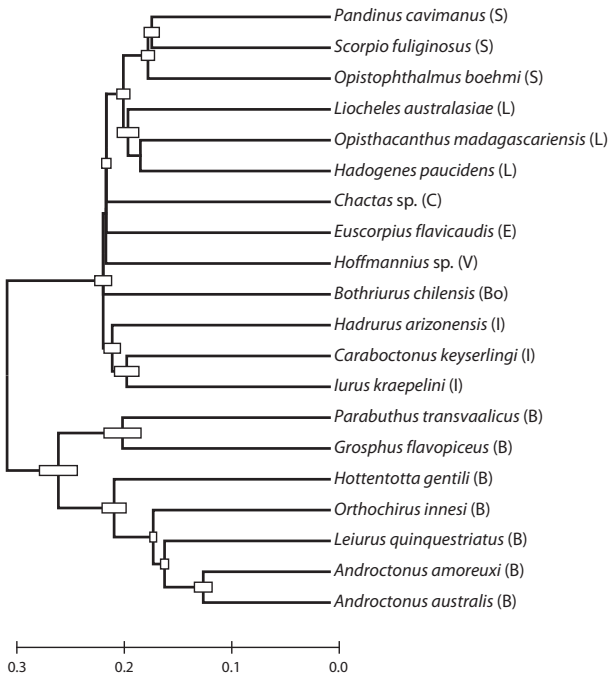

Fig. 4 Linearized tree with branch lengths based on 12S, 16S and CO1 sequences. Phylogenetic independent contrast calculations (Table 4) were based on this phylogram.

particularly those in cluster a1, correspond to the psammophilous ecomorphotype of Polis (1990). The taxa in this cluster are all desert-dwelling scorpions, although *Hottentotta gentili* tends to favor oases (Sousa et al. 2011). Clusters a2 and a3 also contain mostly species inhabiting dry areas, except for the Mediterranean *Iurus* and the Malagasy *Grosphus*. The species of clusters a2 and a3 are to a lesser extent psammophilous and/or vagrant. Cluster a consists mostly of species from the family Buthidae, with the exception of *Iurus*, *Hadrurus* and *Hoffmannius*. Since the Buthidae is the most basal family included in this study, we cannot conclude that these other taxa have evolved this chela morphotype independently or merely maintained the basal condition.

Cluster b contains at least two distinct ecomorphotypes: the fossorial type (b1) and the infrasaxicolous and corticolous types (b2). The infrasaxicolous and corticolous types in cluster 2b have relatively shorter movable fingers. This may be due to the dorso-ventral flattening that enables these species to live in the tight spaces between rocks, in rock cracks and under bark. A dorso-ventral flattening of the chela would reduce the space available for muscle dorsally in the plane of the rotation of the movable finger. The bulk of the muscle is therefore placed more proximally, toward the base of the manus. The muscle-filled part of the manus is relatively longer, conversely making the relative length of the movable finger shorter. The dorso-ventral restriction also reduces the possible length of the in-lever of the movable finger, which may explain the difference ($P = 0.035$; Table 3) in the mechanical advantage between cluster b1 and b2. The fossorial species in cluster b1 are not limited dorso-ventrally and have the highest chelae, with a mechanical advantage favoring high forces. Although such a lever system would reduce closing speed if muscle fibers were to contract at a constant rate (Arnold et al. 2011), this may not make these scorpions slower in closing their chelae.

Table 4 Phylogenetically independent contrasts. Values below the diagonal are Pearson correlation coefficients, values above the diagonal are the corresponding *P*-values. Correlation coefficients with a *P*-value < 0.05 are marked in bold. *P*-values above 0.05 are in grey. Correlation coefficients that result from correlation of non-independent variables are in brackets. All non-ratio and non-angle values were $\log_{10}$-transformed.

Pearson correlation coefficients	1	2	3	4	5	6	7	8	9	10	11	12	13
1 Mean Von Mises stress		<1e−4	0.158	0.123	0.001	<1e−4	0.014	<1e−4	<1e−4	<1e−4	0.280	0.557	0.072
2 Strain energy	**(0.96)**		0.542	0.472	<1e−3	<1e−4	0.010	<1e−4	<1e−4	<1e−4	0.126	0.719	0.056
3 Absolute prosoma length	0.35	0.15		<1e−4	0.806	0.946	0.520	0.708	0.696	0.913	0.429	0.985	0.502
4 Absolute chela length	0.38	0.18	**0.92**		0.482	0.759	0.718	0.707	0.599	0.909	0.162	0.556	0.300
5 Standardized width	**−0.71**	**−0.74**	−0.06	−0.18		<1e−4	0.339	<1e−3	0.001	0.003	0.167	0.792	0.568
6 Standardized height	**−0.84**	**−0.91**	0.02	−0.08	**0.85**		0.096	<1e−3	<1e−4	<1e−4	0.044	0.807	0.200
7 Standardized out-lever length	**0.57**	**0.59**	0.16	0.09	−0.24	−0.4		0.020	0.001	<1e−3	0.122	0.094	0.005
8 Aspect ratio chela	**0.81**	**0.89**	0.1	0.1	**(−0.78)**	**(−0.84)**	**0.54**		<1e−4	<1e−4	0.162	0.486	0.173
9 Mechanical advantage	**0.9**	**0.94**	0.1	0.13	**−0.71**	**−0.87**	**(0.72)**	**0.89**		<1e−3	0.099	0.442	0.027
10 Ratio finger length/ distance LJ-MJ	**0.83**	**0.92**	−0.03	−0.03	**−0.67**	**−0.84**	**(0.75)**	**0.86**	**(0.94)**		0.039	0.186	0.003
11 Curvature of movable finger	0.27	0.37	−0.2	−0.34	−0.34	**−0.48**	0.38	0.34	0.4	0.49		0.856	0.411
12 Angle in-lever/out-lever	−0.15	−0.09	0	0.15	0.07	−0.06	−0.41	−0.18	−0.19	−0.33	−0.05		<1e−3
13 Angle out-lever/axis of rotation	0.43	0.46	−0.17	−0.26	−0.14	−0.32	**0.63**	0.34	**0.52**	**(0.66)**	0.21	**−0.74**	

The high chelae allow the muscle fibers to be much longer, and longer muscle fibers contract over a longer distance than shorter ones per unit of time, which may hypothetically partly offset the reduction in closing speed caused by the mechanical advantage of the lever system. The scorpions in cluster b1 are mostly fossorial species which use their strong chelae for burrowing in hard soil. The scorpions of cluster b2 do not need their relatively strong chelae to dig, but it has been suggested that some members of this clade are durophagous. In particular, *Hadogenes* has been known to prey upon hard-shelled prey such as millipedes and even snails (Newlands, 1978).

The mean Von Mises stress is significantly lower in the more robust chelae morphologies of cluster b. This indicates that under maximal defensive loadings, these chelae are less likely to fail than those of cluster a. The same pattern can be seen for the strain energy, indicating that these chela shapes also deform less. The size-corrected FEA analysis allows the comparison of the effect of shape alone on chela performance. Some of the more extreme chela shapes differ greatly in performance; the bending energy in *Leiurus* is nearly 100 times higher than that in *Scorpio*, and the mean stress more than 10 times higher. These differences can be attributed to shape alone, making chela shape a very important factor in the performance of the chela. To make models comparable and isolate the effect of shape, the material characteristics (Young's module and Poisson's ratio) of the cuticula were set to be the same in all species. This assumption may well be idealistic, as even within a single specimen, cuticula hardness is known to vary widely (Schofield, 2001). Due to application of the total load in several point loads, local stress may have become artificially high. This consideration necessitated our disregarding maximum Von Mises stress as a performance variable.

The lack of a robust molecular phylogenetic hypothesis for the high-level relationships between scorpions makes it hard to make any statements about the independent evolution of ecomorphotypes. It is well known that chela shape can vary widely within scorpion families, such as the Buthidae and Vaejovidae (Stockmann & Ythier, 2010). Also in our clustering analysis, members of the same family (Iuridae) were present in different clusters. This suggests chela shape may well be a homoplastic character. Since changes in the overall shape of the chela may change the relative position of taxonomic characters (Prendini, 2000), systematists using morphological characters of the chela, such as the relative positions of the trichobothria, may need to test for the independence of their characters from the overall chela shape parameters which correlate highest with performance, such as height, width, and relative finger length. As only relatively fast-evolving mitochondrial genes were used to infer branch lengths, the branch lengths used to calculate the phylogenetically independent contrasts may cause an underestimation of the rate of evolution in the basal part of the tree. However, the PIC method analysis has been shown to be a robust method in relation to branch length distributions (Diaz-Uriarte & Garland, 1996; Ackerly, 2000).

Concluding remarks

Our work presents the first mechanical models for the computational assessment of performance of the scorpion chelae, and allows chela shape types to be used as an approximation for performance. Despite the limited number of taxa included, our results clearly show that more elongate chelae experience higher stresses and deformations compared with more robust chelae. This makes these chelae less suitable for tasks that require the chela to perform near its maximum, such as defense, subduing of hard prey, and burrowing. This may be why scorpions with slender chelae use their sting more in the incapacitation of prey (Stahnke, 1966; McCormick & Polis, 1990).

Acknowledgements

We thank Arendo Flipse for supplying several of the scorpions. Thanks to Pedro Sousa for identifying the specimens. We very much appreciate access to the Skyscan CT scanner that was provided by Tim Cox and the team of the small animal tomography facility in Seattle, WA, USA. This work was supported by an FCT I&D grant to A.vdM. (PTDC/BIA-BEC/104644/2008). A.vdM. was supported by FCT postdoctoral fellowship SFRH/BPD/48042/2008 and T.K. by the funding initiative Evolutionary Biology of the Volkswagen Foundation (I 84/206). We are grateful for the comments of two anonymous reviewers which improved the manuscript.

References

Ackerly DD (2000) Taxon sampling, correlated evolution, and independent contrasts. *Evolution* **54**, 1480–1492.

Alexander A (1959) A survey of the biology of scorpions of South Africa. *Afr Wildl* **13**, 99–106.

Arnold AS, Richards CT, Ros IG, et al. (2011) There is always a trade-off between speed and force in a lever system: comment on McHenry (2010). *Biol Lett* **7**, 878–879.

Bruford MW, Hanotte O, Brookfield JFY, et al. (1992) Single-locus and multilocus DNA fingerprint. In: *Molecular Genetic Analysis of Populations: A Practical Approach* (ed. Hoezel AR), pp. 225–270. Oxford: IRL Press.

Diaz-Uriarte R, Garland T (1996) Testing hypotheses of correlated evolution using phylogenetically independent contrasts: sensitivity to deviations from Brownian motion. *Syst Biol* **45**, 27–47.

Dumont ER, Grosse IR, Slater GJ (2009) Requirements for comparing the performance of finite element models of biological structures. *J Theor Biol* **256**, 96–103.

Dunlop JA, Tetlie OE, Prendini L (2008) Reinterpretation of the Silurian scorpion *Proscorpius osborni* (Whitfield): integrating data from paleozoic and recent scorpions. *Palaeontology* **51**, 303–320.

Edgar RC (2004) MUSCLE: multiple sequence alignment with high accuracy and high throughput. *Nucleic Acids Res* **32**, 1792–1797.

Fet V, Sissom WD, Lowe G, et al. (2000) *Catalog of the Scorpions of the World (1758–1998)*. New York: New York Entomological Society.

Fet V, Neff D, Graham MR, et al. (2003) Metasoma of *Orthochirus* (Scorpiones, Buthidae): are scorpions evolving a new sensory organ? *Rév Ibér Arachnol* **8**, 69–72.

Folmer O, Black M, Hoeh W, et al. (1994) DNA primers for amplification of mitochondrial cytochrome c oxidase subunit I from diverse metazoan invertebrates. *Mol Mar Biol Biotechnol* **3**, 294–299.

Gantenbein B, Kropf C, Largiadèr CR, et al. (2000) Molecular and morphological evidence for the presence of a new buthid taxon (Scorpiones: Buthidae) on the island of Cyprus. *Rev Suisse Zool* **107**, 213–232.

Gilai A, Parnas I (1970) Neuromuscular physiology of the closer muscles in the pedipalp of the scorpion *Leiurus quinquestriatus*. *J Exp Biol* **52**, 325–344.

Govindarajan S, Rajulu GS (1974) Presence of resilin in a scorpion *Palamnaeus swammerdami* and its role in the food-capturing and sound-producing mechanisms. *Experientia* **30**, 908–909.

Guindon S, Gascuel O (2003) A simple, fast, and accurate algorithm to estimate large phylogenies by maximum likelihood. *Syst Biol* **52**, 696–704.

Herrel A, Spithoven L, Van Damme R, et al. (1999) Sexual dimorphism of head size in *Gallotia galloti*: testing the niche divergence hypothesis by functional analysis. *Funct Ecol* **13**, 289–297.

Lamoral BH (1979) The scorpions of Namibia (Arachnida: Scorpionida). *Ann Natal Mus* **23**, 497–784.

McCormick SJ, Polis GA (1990) Prey, predators, and parasites. In: *The Biology of Scorpions* (ed. Polis GA), pp. 294–320. Palo Alto: Stanford University Press.

McHenry MJ (2011) There is no trade-off between force and velocity in a dynamic lever system. *Biol Lett* **7**, 384–386.

Newlands G (1969) Scorpion defensive behaviour. *Afr Wildl* **23**, 147–153.

Newlands G (1972) Ecological adaptations of Kruger National Park scorpionids (Arachnida: Scorpionides). *Koedoe* **15**, 37–48.

Newlands G (1978) Arachnida (except Acari). In: *Biogeography and Ecology of Southern Africa* (ed. Werger MJA), pp. 677–684. The Hague: Junk.

Polis GA (1990) Ecology. In: *The Biology of Scorpions* (ed. Polis GA), pp. 247–293. Palo Alto: Stanford University Press.

Posada D (2008) jModelTest: phylogenetic model averaging. *Mol Biol Evol* **25**, 1253–1256.

Prendini L (2000) Phylogeny and classification of the superfamily Scorpionoidea Latreille 1802 (Chelicerata, Scorpiones): an exemplar approach. *Cladistics* **16**, 1–78.

Prendini L, Wheeler WC (2005) Scorpion higher phylogeny and classification, taxonomic anarchy, and standards for peer review in online publishing. *Cladistics* **21**, 446–494.

R Development Core Team (2011) *R: A Language and Environment for Statistical Computing*. Vienna: R Foundation for Statistical Computing. 011, http://www.R-project.org.

Ronquist F, Huelsenbeck JP (2003) MrBayes version 3.0: Bayesian phylogenetic inference under mixed models. *Bioinformatics* **19**, 1572–1574.

Schofield RMS (2001) Metals in cuticular structures. In: *Scorpion Biology and Research* (eds Brownell P, Polis GA), pp. 234–256. New York: Oxford University Press.

Sensenig AT, Shultz JW (2004) Elastic energy storage in the pedipalpal joints of scorpions and sun-spiders (Arachnida, Scorpiones, Solifugae). *J Arachnol* **32**, 1–10.

Simon C, Frati F, Beckenbach A, et al. (1994) Evolution, weighting, and phylogenetic utility of mitochondrial gene sequences and a compilation of conserved polymerase chain reaction primers. *Ann Entomol Soc Am* **87**, 651–701.

Snodgrass RE (1952) *A Textbook of Arthropod Anatomy*. Ithaca: Cornell University Press.

Sousa P, Froufe E, Harris DJ, et al. (2011) Genetic diversity of Maghrebian *Hottentotta* (Scorpiones: Buthidae) scorpions based on CO1: new insights on the genus phylogeny and distribution. *Afr Invertebr* **52**, 135–143.

Stahnke HL (1966) Some aspects of scorpion behavior. *Bull South Calif Acad Sci* **65**, 65–80.

Stockmann R, Ythier E (2010) *Scorpions of the World*. Verrières-le-Bruisson, France: N.A.P Editions.

Tamura K, Peterson D, Peterson N, et al. (2011) MEGA5: molecular evolutionary genetics analysis using maximum likelihood, evolutionary distance, and maximum parsimony methods. *Mol Biol Evol*, **28**, 2731–2739.

Van der Meijden A, Herrel A, Summers A (2010) Comparison of chela size and pincer force in scorpions; getting a first grip. *J Zool* **280**, 319–325.

Vincent JFV, Wegst UGK (2004) Design and mechanical properties of insect cuticle. *Arthropod Struct Dev* **33**, 187–199.

Webb CO, Ackerly DD, Kembel SW (2008) Phylocom: software for the analysis of phylogenetic community structure and character evolution. *Bioinformatics* **24**, 2098–2100.

Yamada SB, Boulding EG (1998) Claw morphology, prey size selection and foraging efficiency in generalist and specialist shell-breaking crabs. *J Exp Mar Biol Ecol* **220**, 191–211.

Supporting Information

Additional Supporting Information may be found in the online version of this article:

Table S1. Sensitivity of Von Mises stress and strain energy to mesh size in the smallest specimen, Orthochirus innesi. Note that mean Von Mises stress and strain energy are insensitive to mesh size.

As a service to our authors and readers, this journal provides supporting information supplied by the authors. Such materials are peer-reviewed and may be re-organized for online delivery, but are not copy-edited or typeset. Technical support issues arising from supporting information (other than missing files) should be addressed to the authors.